ANZIAM J. 62(2020), 42–61
doi:10.1017/S1446181120000073

A MODIFIED IMMERSED FINITE VOLUME ELEMENT METHOD FOR ELLIPTIC INTERFACE PROBLEMS

Q. WANG[1] and Z. ZHANG[2]

(Received 11 October, 2019; accepted 1 March, 2020; first published online 13 May 2020)

Abstract

This paper presents a new immersed finite volume element method for solving second-order elliptic problems with discontinuous diffusion coefficient on a Cartesian mesh. The new method possesses the local conservation property of classic finite volume element method, and it can overcome the oscillating behaviour of the classic immersed finite volume element method. The idea of this method is to reconstruct the control volume according to the interface, which makes it easy to implement. Optimal error estimates can be derived with respect to an energy norm under piecewise H^2 regularity. Numerical results show that the new method significantly outperforms the classic immersed finite volume element method, and has second-order convergence in L^∞ norm.

2020 *Mathematics subject classification*: 65N08.

Keywords and phrases: modified, control volume, interface problems, Cartesian mesh.

1. Introduction

We consider the following second-order elliptic interface problem:

$$\begin{aligned} -\nabla \cdot (\beta(x)\nabla u) &= f \quad \text{in } \Omega^- \cup \Omega^+, \\ u|_{\partial\Omega} &= 0, \end{aligned} \tag{1.1}$$

where $f \in L^2(\Omega)$, $u \in H_0^1(\Omega)$, and $\Omega \subset R^2$ is divided by a C^2 interface Γ into two disjoint subdomains Ω^+ and Ω^-. The diffusion coefficient $\beta(x)$ has a finite discontinuity across the interface Γ, and it is assumed to be a piecewise constant function defined by

$$\beta(x) = \begin{cases} \beta^- & x = (x_1, x_2) \in \Omega^- \\ \beta^+ & x = (x_1, x_2) \in \Omega^+, \end{cases} \tag{1.2}$$

[1]College of Engineering, Nanjing Agricultural University, Nanjing 210031, China; e-mail: wangquanxiang163@163.com.
[2]Jiangsu Key Laboratory for NSLSCS, School of Mathematical Sciences, Nanjing Normal University, Nanjing 210023, China; e-mail: zhangzhiyue@njnu.edu.cn.

such that $\min\{\beta^+,\beta^-\} > 0$. Across the interface Γ, the solution and its flux are assumed to be continuous

$$[u]|_\Gamma = u^+ - u^- = 0, \quad \left[\beta\frac{\partial u}{\partial \mathrm{n}}\right]\Big|_\Gamma = \beta^+\frac{\partial u^+}{\partial \mathrm{n}} - \beta^-\frac{\partial u^-}{\partial \mathrm{n}} = 0, \tag{1.3}$$

where $u^s = u|_{\Omega^s}(s = +, -)$, and n is the normal of Γ. The interface Γ is represented by the zero level-set of a smooth function $\varphi(x)$ which is called a level-set function, and we assume that $\Omega^- = \{x \in \Omega \mid \varphi(x) < 0\}$ and $\Omega^+ = \{x \in \Omega \mid \varphi(x) > 0\}$.

The interface problems arise from many applications in engineering and science, such as multi-phase flows in fluid dynamics [4, 34], cell and tumour growth in mathematical biology [12, 32] and shape optimization [18]. Conventional finite element (FE) methods can solve the elliptic interface problems satisfactorily, provided that solution meshes are tailored to fit the interfaces [2, 3]. However, for moving interface problems, it takes additional cost to reform the mesh at each time step in order to fit the moving interface. In that case, it may be advantageous to use a uniform Cartesian mesh. Quite a few numerical methods in this category have been proposed and studied, such as the immersed boundary method [33], the immersed interface method [24], Nitsche-XFEM method [15] and unfitted penalty finite element method [17]. The immersed finite element (IFE) methods are a particular class of finite element methods based on Cartesian meshes [22, 27, 28, 31]. The basic idea of the IFE method is to employ standard finite element functions on noninterface elements, and modify the approximating functions on interface elements, so that the jump conditions (1.3) are locally preserved in a certain sense. But numerical experiments illustrate that the classic IFE method often has much larger pointwise errors over interface elements, and its convergence order decreases slightly in the H^1 norm when the mesh becomes very fine [19, 29]. In addition, the convergence order in the L^∞ norm has the oscillation property.

To overcome the difficulties, the partially penalized immersed finite element (PPIFE) methods are proposed in the literature [1, 19–21, 29]. The penalization terms are added to IFE schemes to deal with the negative impacts caused by the discontinuity in the IFE functions. The PPIFE methods can eliminate the shortcomings of the classic IFE methods, and obtain smaller pointwise errors. Theoretically, it is difficult to prove the coercivity of the PPIFE methods without extra stabilized terms, and piecewise H^3 regularity is needed to establish the optimal convergence with respect to the defined energy norm [29]. Computationally, adding penalized and stabilized terms makes the method hard to implement and has a higher computational cost. The nonconforming rotated-Q1 IFE method without stabilized term is developed [14, 30]. Numerical results demonstrate that the convergence order in the L^∞ norm is approximately second-order. However, the degrees of freedom of the nonconforming IFE method are about twice as much as that of the conforming IFE method on the same mesh.

Due to the local conservation property and other attractive properties, the finite volume element (FVE) method is widely used in computational fluid dynamics (see [5, 7, 13, 25, 37–39] and the references therein). Although the numerical analysis of

https://doi.org/10.1017/S1446181120000073 Published online by Cambridge University Press

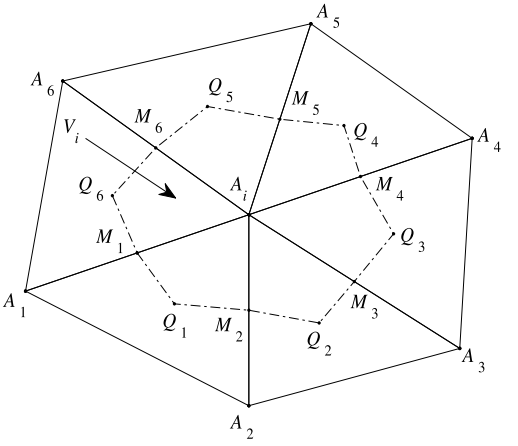

FIGURE 1. Dual element/control volume with barycentre as internal point.

the FVE method is more difficult than that of the FE method, a general framework for analysing the FVE methods has been proposed [8, 9, 11]. To solve the second-order elliptic interface problems efficiently, the immersed finite volume element (IFVE) method is designed [10]. Optimal error estimates in the energy norm are obtained under piecewise H^2 regularity. The bilinear IFVE method for solving the second-order elliptic interface problem is presented by He et al. [16]. The elliptic interface problems with nonhomogeneous jump conditions are solved by the linear IFVE method [41]. To improve the classic IFVE methods, certain stability terms are added on interface elements [36].

A typical finite volume element method uses piecewise constant functions as test functions, and to keep the same dimension for the spaces of the trial functions and test functions, two different partitions of the domain Ω are needed. In Figure 1, the primal partition is made up of the standard triangular elements, and the dual partition is constructed as follows. Let A_i be a node of a triangle, A_j $(j = 1, 2, \ldots, 6)$ the adjacent nodes of A_i, and M_j the midpoint of $\overline{A_jA_i}$. We choose the barycentre Q_j of triangle $\triangle A_jA_iA_{j+1}$ $(A_7 = A_1)$ as the node of the dual mesh. Also, we successively connect M_1, $Q_1, \ldots, M_6$, Q_6, M_1 to form a polygonal region V_i, called a control volume. When the diffusion coefficient is continuous, the dual partition makes the corresponding finite volume element schemes hold optimal L^2 norm convergence order [40]. Numerical results show that optimal convergence order in the L^2 norm can also be obtained for the elliptic interface problems [10, 36, 41]. However, numerical results illustrate that the convergence order in the L^∞ norm has the oscillating behaviour for a large jump of the diffusion coefficients, which is also observed in the IFE methods.

In this paper, a modified immersed finite volume element (MIFVE) method is developed to solve the second-order elliptic interface problems on a Cartesian mesh. The idea is to modify the control volume associated with the interface elements. Specifically, the construction of the control volume for noninterface element is the

https://doi.org/10.1017/S1446181120000073 Published online by Cambridge University Press

same as that of the standard FVE method. For the interface element, the control volume is designed along the interface. Compared with other methods [36], the new method is parameter free and easy to implement, which makes it applicable to other interface problems, such as planar elasticity and Stokes interface problems [35]. Furthermore, the coercivity and optimal error estimates can be derived in an energy norm under piecewise H^2 regularity.

The rest of the paper is organized as follows. In the next section, we introduce some notations, immersed finite element space and modified immersed finite volume element method for the elliptic interface problems. In Section 3, we present some numerical results to confirm our theoretical analysis and efficiency of the new method. The conclusions are summarized in the last section.

2. Some notations and MIFVE schemes

2.1. Some notations and immersed finite element space For the elliptic interface problem described by (1.1) and (1.3), we consider the weak form: find $u \in H_0^1(\Omega)$ such that

$$a(u, v) = (f, v) \quad \text{for all } v \in H_0^1(\Omega), \tag{2.1}$$

where

$$a(u, v) = \int_\Omega \beta \nabla u \cdot \nabla v \, dx, \quad (f, v) = \int_\Omega f v \, dx \quad \text{for all } v \in H_0^1(\Omega).$$

To present error estimates, we define the following function space

$$\tilde{H}^2(\Omega) = \{v \mid v|_{\Omega^s} \in H^2(\Omega^s), s = + \text{ or } -\},$$

equipped with the norm and semi-norm

$$\|v\|^2_{\tilde{H}^2(\Omega)} = \|v\|^2_{H^2(\Omega^+)} + \|v\|^2_{H^2(\Omega^-)},$$

$$|v|^2_{\tilde{H}^2(\Omega)} = |v|^2_{H^2(\Omega^+)} + |v|^2_{H^2(\Omega^-)},$$

where $H^2(\Omega^s) = W_2^2(\Omega^s)$ denotes the usual Sobolev space. Then, we have the following regularity result for the weak solution of the variational problem [3, 6].

THEOREM 2.1. *The variational problem* (2.1) *has a unique solution* $u \in \tilde{H}^2(\Omega) \cap H_0^1(\Omega)$ *which satisfies*

$$\|u\|_{\tilde{H}^2(\Omega)} \le C \|f\|_{L^2(\Omega)}$$

for some constant $C > 0$.

Now we recall the linear IFE space [10, 27, 36]. Let $\mathcal{T}_h = \{T\}$ be a regular triangular grid of Ω with grid size h. We call an element T an interface element, if the interface Γ passes through the interior of T; otherwise, we call T a noninterface element. Without loss of generality [30], we assume that interface elements in $\mathcal{T}_h$ have the following features when the mesh size h is small enough.

https://doi.org/10.1017/S1446181120000073 Published online by Cambridge University Press

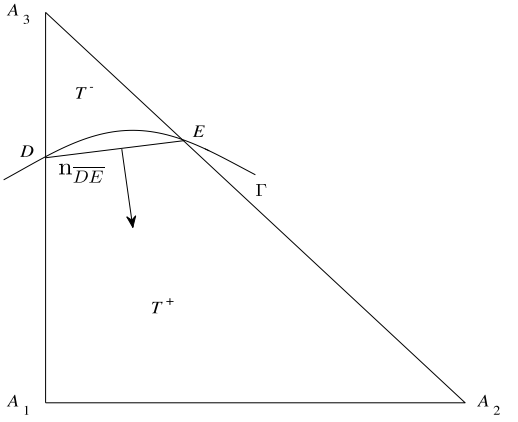

FIGURE 2. A typical interface element.

(H_1) The interface Γ cannot intersect an edge of any element at more than two points, unless the edge is part of Γ.

(H_2) If Γ intersects the boundary of an element at two points, these intersection points must be on different edges of this element.

Note that if Γ continuously intersects an edge of one triangle twice, then the element is a noninterface element. The set of interface elements and the set of the noninterface elements are denoted by $\mathcal{T}_h^i$ and $\mathcal{T}_h^n$, respectively. As a common practice, the interface Γ can be approximated by Γ_h which is composed of all the line segments connecting the intersections of the elements and the interface. Such an approximation does not affect second-order convergence, when $\Gamma \in C^2$ (see [3, 6]). In addition, we use

$$N_h = \{A_i \mid A_i \text{ is a node of element } T \in \mathcal{T}_h\}$$

to denote the set of all nodes of $\mathcal{T}_h$.

For a typical interface element $\triangle A_1A_2A_3$, its geometric configuration is given in Figure 2. Assume that the interface Γ meets the triangle at points D and E, and the straight line $\overline{DE}$ separates T into T^+ and T^-. We then define the shape function to be a piecewise linear polynomial

$$\phi(x) = \begin{cases} \phi^-(x) = a^- x_1 + b^- x_2 + c^- & \text{if } x \in T^- \\ \phi^+(x) = a^+ x_1 + b^+ x_2 + c^+ & \text{if } x \in T^+. \end{cases}$$

The coefficients are chosen such that

$$\phi(A_i) = N_i, \quad i = 1, 2, 3, \tag{2.2}$$

$$\phi^+(D) = \phi^-(D), \quad \phi^+(E) = \phi^-(E), \quad \beta^+ \frac{\partial \phi^+}{\partial \mathrm{n}_{\overline{DE}}} = \beta^- \frac{\partial \phi^-}{\partial \mathrm{n}_{\overline{DE}}}, \tag{2.3}$$

where $N_i, i = 1, 2, 3$ are given nodal values and $\mathrm{n}_{\overline{DE}}$ is the unit normal vector on the line segment $\overline{DE}$. The piecewise linear function $\phi(x)$ on interface element T is

https://doi.org/10.1017/S1446181120000073 Published online by Cambridge University Press

uniquely determined by the six conditions in (2.2)–(2.3), which has been proved by Ewing et al. [10] and Li et al. [26]. We let $\widehat{S}_h(T)$ denote the three-dimensional linear space spanned by these piecewise linear functions. For any $v \in \tilde{H}^2(T)$, we define $I_h v \in \widehat{S}_h(T)$ such that

$$I_h v(A_i) = v(A_i), \quad i = 1, 2, 3,$$

where $A_i, i = 1, 2, 3$ are the vertices of T, and we call $I_h v$ the interpolation of v in $\widehat{S}_h(T)$. For functions in $\widehat{S}_h(T)$, they exactly satisfy a weak flux jump condition on the interface Γ.

LEMMA 2.2. *For an interface element T, every function $\phi \in \widehat{S}_h(T)$ satisfies the flux jump condition on $\Gamma \cap T$ in the following weak sense:*

$$\int_{\Gamma \cap T} \left(\beta^- \frac{\partial \phi^-}{\partial \mathrm{n}} - \beta^+ \frac{\partial \phi^+}{\partial \mathrm{n}} \right) ds = 0.$$

For a noninterface element $T \in \mathcal{T}_h^n$, we use the standard piecewise linear polynomials as local basis functions, and use $\overline{S}_h(T)$ to denote the linear space spanned by the three nodal basis functions on T. Then we use the triangulation $\mathcal{T}_h = \{T\}$ to define the immersed finite element space $\widehat{S}_h(\Omega)$ as the set of functions such that

$$\begin{cases} \phi|_T \in \overline{S}_h(T) & \text{if } T \in \mathcal{T}_h^n \\ \phi|_T \in \widehat{S}_h(T) & \text{if } T \in \mathcal{T}_h^i \\ \phi & \text{is continuous at all nodes} \\ \phi(x) = 0 & \text{if } x \text{ is a node on } \partial\Omega. \end{cases}$$

Now we have the following estimate that was proved by Li et al. [26].

LEMMA 2.3. *For every $v \in \tilde{H}^2(\Omega) \cap H_0^1(\Omega)$, there exists a constant $C > 0$ such that its interpolation in the space $\widehat{S}_h(\Omega)$ has the error bound*

$$\|v - I_h v\|_{L^2(\Omega)} + h \left(\sum_{T \in \mathcal{T}_h} \|v - I_h v\|_{H^1(T)}^2 \right)^{1/2} \le C h^2 \|v\|_{\tilde{H}^2(\Omega)}.$$

2.2. MIFVE method Since the FVE method involves two different function spaces, it is more difficult than finite element method to derive the error estimates. In recent years, some approaches are established for analysing the FVE method applied to second-order elliptic problems with continuous diffusion coefficients [8, 9, 11]. The basic idea is to treat the FVE method a perturbation of the finite element method. So first, we present some results about the IFE method for the elliptic interface problems in the following.

Now we describe the IFE method for the elliptic interface problems (1.1)–(1.3): find $u_h \in \widehat{S}_h(\Omega)$ such that

$$a_h(u_h, v_h) = (f, v_h) \quad \text{for all } v_h \in \widehat{S}_h(\Omega), \tag{2.4}$$

where

$$a_h(u_h, v_h) = \sum_{T \in \mathcal{T}_h} \int_T \beta \nabla u_h \cdot \nabla v_h \, dx \quad \text{for all } v_h \in \widehat{S}_h(\Omega).$$

https://doi.org/10.1017/S1446181120000073 Published online by Cambridge University Press

To show the boundedness and coercivity of the bilinear form $a_h(\cdot,\cdot)$, we define the following energy norm

$$\|v_h\|_h = \sqrt{a_h(v_h, v_h)} = \sqrt{\sum_{T\in\mathcal{T}_h} \|v_h\|_{h,T}^2} \quad \text{for all } v_h \in \widehat{S}_h(\Omega),$$

where $\|v_h\|_{h,T}^2 = \int_T \beta \nabla v_h \cdot \nabla v_h \, dx$. Then we have the following lemma.

Lemma 2.4. *There exist two positive constants C_0, C_1 such that for any $u_h, v_h \in \widehat{S}_h(\Omega)$,*

$$|a_h(u_h, v_h)| \le C_0 \|u_h\|_h \|v_h\|_h, \quad a_h(u_h, u_h) \ge C_1 \|u_h\|_h^2.$$

Next, we derive the error bound of IFE solutions for completeness.

Theorem 2.5. *Let $u \in \tilde{H}^2(\Omega) \cap H_0^1(\Omega)$, $u_h \in \widehat{S}_h(\Omega)$ be the solutions of (2.1) and (2.4), respectively. Then there exists a constant C such that*

$$\|u - u_h\|_h \le Ch \|u\|_{\tilde{H}^2(\Omega)}. \tag{2.5}$$

Proof. From the weak forms (2.1) and (2.4),

$$a_h(u - w_h, v_h) = a_h(u_h - w_h, v_h) \quad \text{for all } v_h, w_h \in \widehat{S}_h(\Omega).$$

Taking $v_h = u_h - w_h$ and using the coercivity of $a_h(\cdot,\cdot)$ yield

$$\begin{aligned}
C_1\|u_h - w_h\|_h^2 &\le a_h(u_h - w_h, u_h - w_h) \\
&= a_h(u - w_h, u_h - w_h) \\
&= \sum_{T\in\mathcal{T}_h} \int_T \beta \nabla(u - w_h) \cdot \nabla(u_h - w_h)\, dx \\
&\le \Big(\sum_{T\in\mathcal{T}_h} \|\beta^{1/2}\nabla(u - w_h)\|_{L^2(T)}^2 \Big)^{1/2} \Big(\sum_{T\in\mathcal{T}_h} \|\beta^{1/2}\nabla(u_h - w_h)\|_{L^2(T)}^2 \Big)^{1/2} \\
&\le C_2 \|\nabla(u - w_h)\|_{L^2(\Omega)}^2 + \frac{C_1}{2}\|u_h - w_h\|_h^2.
\end{aligned}$$

Then, taking $w_h = I_h u$ and using the Lemma 2.3,

$$\|u_h - w_h\|_h \le C_3 h \|u\|_{\tilde{H}^2(\Omega)}.$$

Finally, we obtain the desired error estimate (2.5) from the triangle inequality

$$\begin{aligned}
\|u - u_h\|_h &\le \|u - I_h u\|_h + \|u_h - I_h u\|_h \\
&\le Ch \|u\|_{\tilde{H}^2(\Omega)}.
\end{aligned}$$

□

Now we present the formulation of the MIFVE method. For the noninterface element, the construction of dual partition is the same as the standard FVE method. Let M_1, M_2 and M_3 be the midpoints of the $\triangle A_1A_2A_3$. We take the barycentre Q in $\triangle A_1A_2A_3$, and connect Q to the points M_1, M_2 and M_3, respectively. For the interface

https://doi.org/10.1017/S1446181120000073 Published online by Cambridge University Press

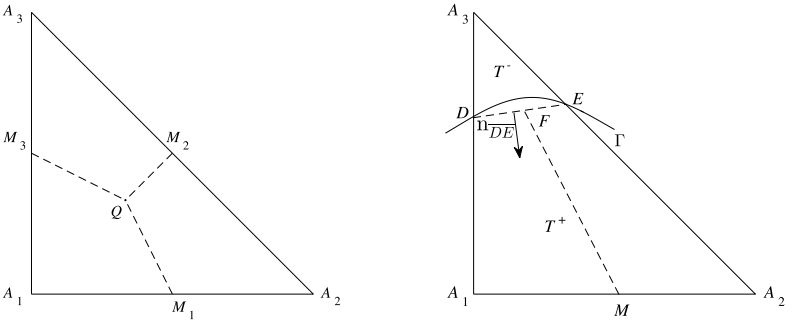

FIGURE 3. Non-interface element (left) and interface element (right).

element, we will design the dual partition along the interface Γ_h. Let M and F be the midpoints of $\overline{A_1A_2}$ and $\overline{DE}$, respectively. Then connecting F to the point M, we get the dual grid on the interface element. Their geometric configurations are given in Figure 3. We call V_i a control volume or a dual element centred at A_i which is a vertex of element T. At last, the dual partition $\mathcal{T}_h^*$ corresponding to the primal partition $\mathcal{T}_h$ is defined as the collection of all these control volumes.

Let

$$S_h^* = \{v \in L^2(\Omega) \mid v|_V \text{ is constant for all } V \in \mathcal{T}_h^* \text{ and } v|_{\partial\Omega} = 0\}$$

be the test function space defined on the dual mesh $\mathcal{T}_h^*$, and $I_h^* : \widehat{S}_h(\Omega) \to S_h^*$ be the piecewise constant interpolation operator such that

$$I_h^* u(x) = u(A_j) \quad \text{for all } x \in V_j, A_j \in N_h.$$

By the interpolation theorem of Sobolev spaces, for $v \in \hat{S}_h(\Omega)$

$$\|v - I_h^* v\|_{L^2(\Omega)} \le Ch|v|_{H^1(\Omega)}.$$

Then the MIFVE schemes for (1.1) are defined as follows: find $u_h \in \widehat{S}_h(\Omega)$ such that

$$\tilde{a}_h(u_h, I_h^* v_h) = (f, I_h^* v_h) \quad \text{for all } v_h \in \widehat{S}_h(\Omega), \tag{2.6}$$

where

$$\tilde{a}_h(u_h, I_h^* v_h) = -\sum_{V_i} I_h^* v_h \int_{\partial V_i} \beta \nabla u_h \cdot \mathrm{n}\, ds.$$

In fact, the bilinear form $\tilde{a}_h(\cdot, I_h^* \cdot)$ can be treated as a perturbation of the bilinear form $a_h(\cdot, \cdot)$. The corresponding results are presented in the following lemmas (see [10, 36, 41]).

LEMMA 2.6. *Assume that $u_h, v_h \in \widehat{S}_h(\Omega)$; then*

$$a_h(u_h, v_h) = \tilde{a}_h(u_h, I_h^* v_h) + E_h(u_h, v_h),$$

https://doi.org/10.1017/S1446181120000073 Published online by Cambridge University Press

where

$$E_h(u_h, v_h) = \sum_{T\in\mathcal{T}_h^i} \int_{\partial T} (\beta \nabla u_h \cdot \mathrm{n})(v_h - I_h^* v_h)\, ds,$$

and

$$|E_h(u_h, v_h)| \le Ch \|u_h\|_h \|v_h\|_h.$$

LEMMA 2.7. *There exist two constants $C_0, C_1 > 0$ independent of the interface location and $h_0 > 0$ such that for all $0 < h \le h_0$,*

$$|\tilde{a}_h(u_h, I_h^* v_h)| \le C_0 \|u_h\|_h \|v_h\|_h, \quad \tilde{a}_h(v_h, I_h^* v_h) \ge C_1 \|v_h\|_h^2.$$

LEMMA 2.8. *There exist constants $C > 0$ and $h_0 > 0$ such that for all $0 < h \le h_0$,*

$$\|u_h\|_h \le C \|f\|_{L^2(\Omega)}.$$

LEMMA 2.9. *For any $u \in \tilde{H}^2(\Omega) \cap H_0^1(\Omega)$ and $v_h \in \widehat{S}(\Omega)$, there exists a constant C independent of h and interface location such that*

$$|F_h(u, v_h)| \le Ch \|u\|_{\tilde{H}^2(\Omega)} \|v_h\|_h,$$

where

$$F_h(u, v_h) = \sum_{T\in\mathcal{T}_h} \int_{\partial T} \beta \frac{\partial u}{\partial \mathrm{n}} v_h\, ds.$$

Using the above lemmas, we can derive the error bound for MIFVE solutions generated by (2.6).

THEOREM 2.10. *Assume that $\mathcal{T}_h$ is regular, $u \in \tilde{H}^2(\Omega) \cap H_0^1(\Omega)$ and $u_h \in \widehat{S}(\Omega)$ are the solutions of (2.1) and (2.6), respectively, then there exists a constant $C > 0$ such that*

$$\|u - u_h\|_h \le Ch(\|u\|_{\tilde{H}^2(\Omega)} + \|f\|_{L^2(\Omega)}). \tag{2.7}$$

PROOF. For $v_h \in \widehat{S}_h(\Omega)$,

$$\begin{aligned} a_h(u, v_h) &= \sum_{T\in\mathcal{T}_h} \int_T \beta \nabla u \cdot \nabla v_h\, dx \\ &= \sum_{T\in\mathcal{T}_h} - \int_T v_h \nabla \cdot (\beta \nabla u)\, dx + \int_{\partial T} \beta \frac{\partial u}{\partial \mathrm{n}} v_h\, ds \\ &= (f, v_h) + \sum_{T\in\mathcal{T}_h} \int_{\partial T} \beta \frac{\partial u}{\partial \mathrm{n}} v_h\, ds. \end{aligned}$$

From Lemma 2.6 we obtain

$$\begin{aligned} a_h(u - u_h, v_h) &= a_h(u, v_h) - a_h(u_h, v_h) \\ &= (f, v_h) + F_h(u, v_h) - \tilde{a}_h(u_h, I_h^* v_h) - E_h(u_h, v_h) \\ &= (f, v_h - I_h^* v_h) + F_h(u, v_h) - E_h(u_h, v_h). \end{aligned}$$

https://doi.org/10.1017/S1446181120000073 Published online by Cambridge University Press

For $w_h \in \widehat{S}_h(\Omega)$, letting $v_h = u_h - w_h$ and using the coercivity of $\tilde{a}_h(\cdot, I_h^*\cdot)$ yield

$$\begin{aligned} C_1\|v_h\|_h^2 &\le |\tilde{a}_h(u_h - w_h, I_h^* v_h)| \\ &= |\tilde{a}_h(u - w_h, I_h^* v_h)| \\ &= |a_h(u - w_h, v_h) - E_h(u - w_h, v_h)| \\ &= |(f, v_h - I_h^* v_h) + F_h(u, v_h) - E_h(w_h, v_h) - E_h(u - w_h, v_h)| \\ &= |R_1 + R_2 + R_3 + R_4|, \end{aligned}$$

where $R_1 = (f, v_h - I_h^* v_h)$, $R_2 = F_h(u, v_h)$, $R_3 = -E_h(w_h, v_h)$ and $R_4 = -E_h(u - w_h, v_h)$. For R_1,

$$\begin{aligned} |R_1| &\le \sum_{T\in\mathcal{T}_h} (f, v_h - I_h^* v_h)_T \\ &\le C_2 h \sum_{T\in\mathcal{T}_h} \|f\|_{L^2(T)}\|v_h\|_{h,T} \\ &\le C_3 h\|f\|_{L^2(\Omega)}\|v_h\|_h. \end{aligned}$$

Using Lemma 2.6 and 2.9, R_2, R_3 and R_4 can be bounded by as follows:

$$\begin{aligned} |R_2| &\le C_4 h\|u\|_{\tilde{H}^2(\Omega)}\|v_h\|_h, \\ |R_3| &\le C_5 h\|w_h\|_h\|v_h\|_h, \\ |R_4| &\le C_6 h\|u - w_h\|_h\|v_h\|_h. \end{aligned}$$

Putting the bounds for R_i, $i = 1, 2, 3, 4$,

$$\|v_h\|_h^2 \le C_7 h(\|f\|_{L^2(\Omega)} + \|u\|_{\tilde{H}^2(\Omega)} + \|u - w_h\|_h)\|v_h\|_h.$$

Taking $w_h = I_h u$ and using Lemma 2.3,

$$\|u_h - I_h u\|_h \le C_8 h(\|f\|_{L^2(\Omega)} + \|u\|_{\tilde{H}^2(\Omega)}).$$

From Lemma 2.3 and triangle inequality, we have

$$\begin{aligned} \|u - u_h\|_h &\le \|u - I_h u\|_h + \|u_h - I_h u\|_h \\ &\le Ch(\|f\|_{L^2(\Omega)} + \|u\|_{\tilde{H}^2(\Omega)}). \end{aligned}$$

This completes the proof. □

Remark 2.11. The estimate given in (2.7) is derived under piecewise H^2 regularity. If the full piecewise H^2 regularity is not achieved, such as $u \in \tilde{H}^{3/2}$, the R_2 can be bounded by $O(h)$ [23]. However, the analysis requires the interpolation error estimates for IFE functions based on $u \in \tilde{H}^{3/2}$, which is the barrier for the error estimate.

https://doi.org/10.1017/S1446181120000073 Published online by Cambridge University Press

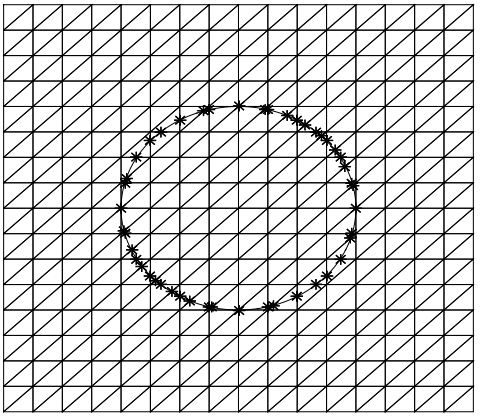

FIGURE 4. A typical Cartesian mesh for Example 3.1.

3. Numerical examples

In this section, we will provide four numerical examples to confirm our theoretical results and demonstrate the features of the modified immersed finite volume element method for the elliptic interface problems. To illustrate the accuracy of the proposed method, we estimate the experimental order (EO) of accuracy by computing the logarithmic ratios of the errors between two successive refined meshes, that is,

$$\mathrm{EO} = \log_2(\|e_{2h}\|/\|e_h\|), \quad e_h = u_h - u,$$

where u_h is the numerical solution with space step size h and u is the analytical solution. The rate should be close to two for second-order accuracy. We consider the elliptic interface problem (1.1)–(1.3), except when the nonhomogeneous boundary condition $u_{|\partial\Omega} = g$ is used. Let the solution domain Ω be the square domain $(-1,1)\times(-1,1)$ which is partitioned into $2N^2$ triangles with mesh size $h = 2/N$.

EXAMPLE 3.1. The interface Γ is a circle centred at the origin with a radius $r_0 = 0.5$ [10, 19]. The level-set function $\varphi(x) = x_1^2 + x_2^2 - 0.25$. The boundary condition g and the source function f are chosen such that the exact solution is

$$u(x) = \begin{cases} \dfrac{r^3}{\beta^-} & \text{if } x \in \Omega^- \\ \dfrac{r^3}{\beta^+} + \left(\dfrac{1}{\beta^-} - \dfrac{1}{\beta^+}\right) r_0^3 & \text{if } x \in \Omega^+, \end{cases}$$

where $r = \sqrt{x_1^2 + x_2^2}$. A typical Cartesian mesh for the interface problem is presented in Figure 4.

The numerical results of our MIFVE method for high coefficient contrasts $(\beta^-,\beta^+) = (1, 10^4)$ and $(\beta^-,\beta^+) = (10^4, 1)$ are reported in Table 1. The MIFVE method converges optimally in the H^1 norm, which validates our error estimates. The data in the table

https://doi.org/10.1017/S1446181120000073 Published online by Cambridge University Press

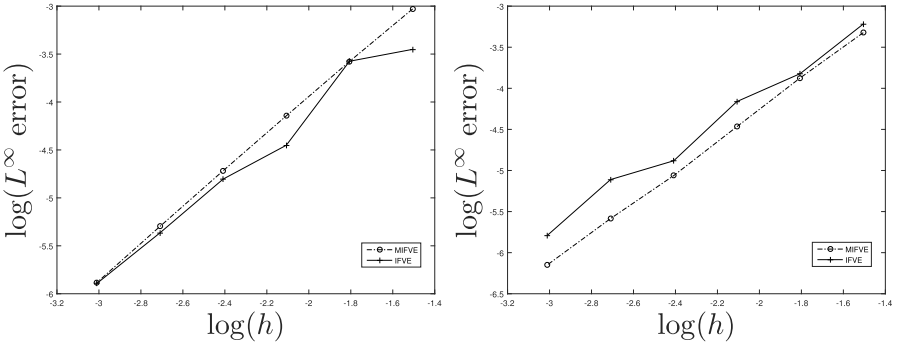

FIGURE 5. The L^∞ error under uniform refinement of the mesh for Example 3.1 with $(\beta^-, \beta^+) = (1, 10^4)$ (left) and $(\beta^-, \beta^+) = (10^4, 1)$ (right).

TABLE 1. Errors of the MIFVE method for Example 3.1 with high coefficient contrasts.

Cases	N	L^∞ error	EO	L^2 error	EO	H^1 error	EO
$\beta^- = 1$	64	9.3550E-04	—	3.3650E-04	—	2.0956E-02	—
$\beta^+ = 10^4$	128	2.6498E-04	1.82	7.6990E-05	2.12	1.0320E-02	1.02
	256	7.1770E-05	1.88	1.8887E-05	2.03	4.9944E-03	1.05
	512	1.9166E-05	1.90	4.7996E-06	1.98	2.4825E-03	1.00
	1024	5.0387E-06	1.93	1.0827E-06	2.15	1.2202E-03	1.02
	2048	1.3058E-06	1.95	2.7199E-07	1.99	6.1216E-04	1.00
$\beta^- = 10^4$	64	4.7553E-04	—	1.3089E-03	—	1.0027E-01	—
$\beta^+ = 1$	128	1.3351E-04	1.83	3.3128E-04	1.98	5.0144E-02	1.00
	256	3.4139E-05	1.97	8.3129E-05	1.99	2.5043E-02	1.00
	512	8.6644E-06	1.98	2.0762E-05	2.00	1.2520E-02	1.00
	1024	2.5988E-06	1.74	5.2366E-06	1.99	6.2563E-03	1.00
	2048	7.0997E-07	1.87	1.3077E-06	2.00	3.1286E-03	1.00

demonstrate a clear second-order accuracy in the L^2 norm. The numerical results also show that the MIFVE solution has the second-order convergence in the L^∞ norm, which is optimal from the viewpoint of polynomial degrees. Similar conclusions can be obtained for small coefficient jumps (for example, $\beta^- = 1$, $\beta^+ = 10$), which are omitted in the paper for the sake of brevity and readability.

In Figure 5, the development of the L^∞ error of MIFVE and IFVE method in the log–log scale versus the mesh size h is shown. The results indicate that the MIFVE solution converges to the exact solution with second-order convergence. But the IFVE solution does not always have the second-order convergence in the L^∞ norm, and it has the oscillation property which is observed in other numerical methods. In other words, the MIFVE method outperforms the IFVE method for the high coefficient contrasts. Additionally, the MIFVE solutions with $N = 64$ for these two contrasting coefficient are plotted in Figure 6.

https://doi.org/10.1017/S1446181120000073 Published online by Cambridge University Press

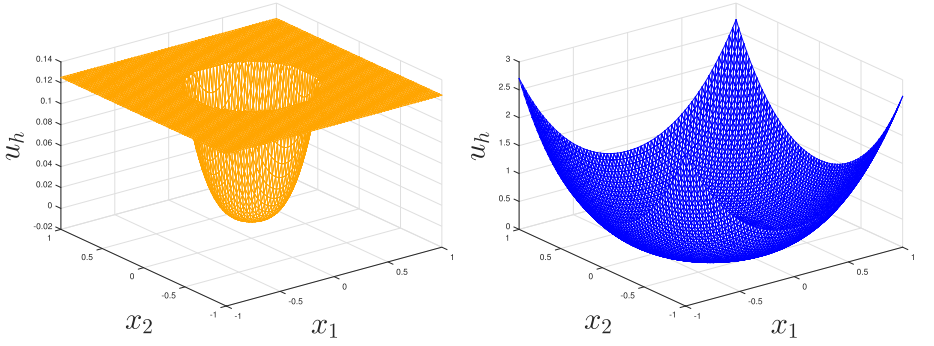

FIGURE 6. MIFVE solutions for Example 3.1 with $(\beta^-, \beta^+) = (1, 10^4)$ (left) and $(\beta^-, \beta^+) = (10^4, 1)$ (right).

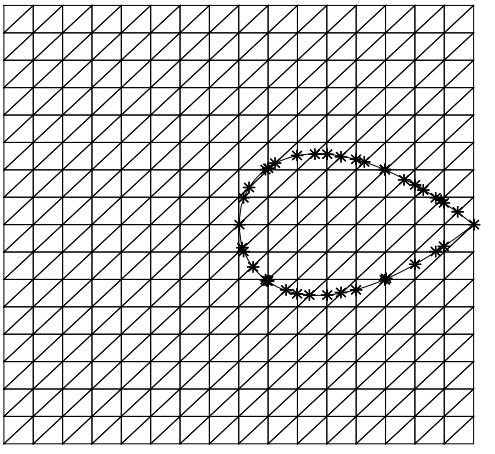

FIGURE 7. A typical Cartesian mesh for Example 3.2.

The efficiency of the MIFVE method is demonstrated in Examples 3.2–3.4. Note that the MIFVE method again shows the optimal convergence behaviour in H^1, L^2 and L^∞ norms. But the IFVE method does not always have the second-order convergence in the L^∞ norm.

EXAMPLE 3.2. We consider the case when the interface has a sharp corner. The level-set function $\varphi(x) = ((x_1 - 1)\tan\theta)^2 x_1 - x_2^2$, where $\theta = 40°$. The exact solution is chosen as

$$u(x) = \begin{cases} \dfrac{\varphi(x)}{\beta^-} & \text{if } x \in \Omega^- \\ \dfrac{\varphi(x)}{\beta^+} & \text{if } x \in \Omega^+. \end{cases}$$

A typical Cartesian mesh for the interface problem is presented in Figure 7. Table 2 shows the error on different grids. In Figure 8, we plot the L^∞ error of MIFVE and

https://doi.org/10.1017/S1446181120000073 Published online by Cambridge University Press

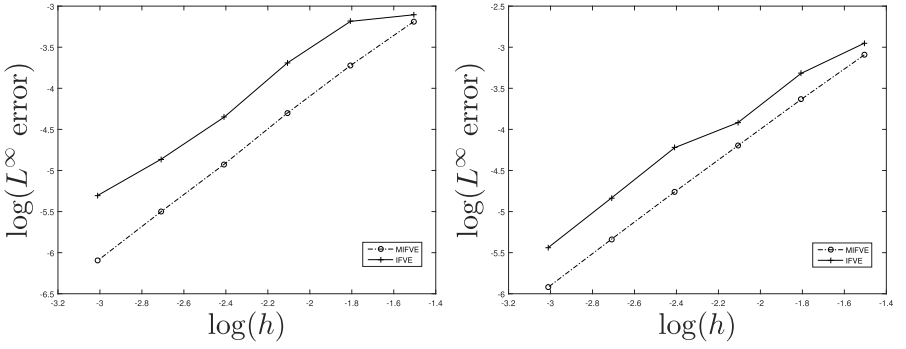

FIGURE 8. The L^∞ error under uniform refinement of the mesh for Example 3.2 with $(\beta^-, \beta^+) = (1, 10^4)$ (left) and $(\beta^-, \beta^+) = (10^4, 1)$ (right).

TABLE 2. Errors of the MIFVE method for Example 3.2 with high coefficient contrasts and $\theta = 40°$.

Cases	N	L^∞ error	EO	L^2 error	EO	H^1 error	EO
$\beta^- = 1$	64	6.4820E-04	—	7.6188E-04	—	7.4978E-02	—
$\beta^+ = 10^4$	128	1.8912E-04	1.78	1.9176E-04	1.99	3.7456E-02	1.00
	256	4.9901E-05	1.92	4.7069E-05	2.03	1.8719E-02	1.00
	512	1.1891E-05	2.06	1.1835E-05	1.99	9.3589E-03	1.00
	1024	3.1475E-06	1.92	2.9477E-06	2.00	4.6787E-03	1.00
	2048	8.0156E-07	1.97	7.3497E-07	2.00	2.3392E-03	1.00
$\beta^- = 10^4$	64	8.0487E-04	—	7.5543E-05	—	1.5454E-02	—
$\beta^+ = 1$	128	2.3135E-04	1.80	2.1058E-05	1.84	7.5756E-03	1.03
	256	6.3518E-05	1.86	4.3745E-06	2.26	3.7250E-03	1.02
	512	1.7388E-05	1.87	1.1555E-06	1.92	1.8595E-03	1.00
	1024	4.6126E-06	1.91	2.7080E-07	2.09	9.2522E-04	1.01
	2048	1.2046E-06	1.94	6.6836E-08	2.02	4.6190E-04	1.00

IFVE method in the log–log scale versus the mesh size h. Figure 9 shows the MIFVE solutions with $N = 64$ for these two contrasting coefficients.

EXAMPLE 3.3. The level-set function $\varphi(x) = x_2 - 3x_1(x_1 - 0.3)(x_1 - 0.8) - 0.34$ [21]. The exact solution is chosen as

$$u(x) = \begin{cases} \dfrac{\varphi(x)}{\beta^-} & \text{if } x \in \Omega^- \\ \dfrac{\varphi(x)}{\beta^+} & \text{if } x \in \Omega^+. \end{cases}$$

A typical Cartesian mesh for the interface problem is presented in Figure 10. Table 3 shows the error on different grids. In Figure 11, we plot the L^∞ error of MIFVE and IFVE method in the log–log scale versus the mesh size h. Figure 12 shows the MIFVE solutions with $N = 64$ for these two contrasting coefficients.

https://doi.org/10.1017/S1446181120000073 Published online by Cambridge University Press

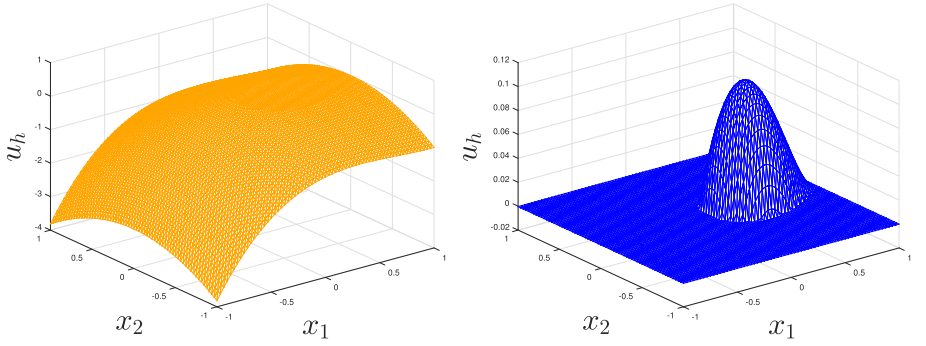

FIGURE 9. MIFVE solutions for Example 3.2 with $(\beta^-, \beta^+) = (1, 10^4)$ (left) and $(\beta^-, \beta^+) = (10^4, 1)$ (right).

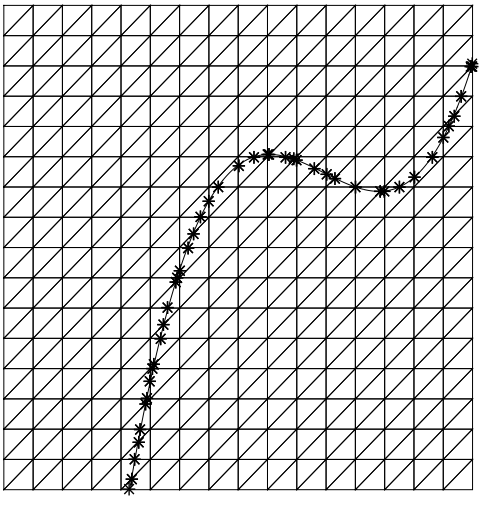

FIGURE 10. A typical Cartesian mesh for Example 3.3.

EXAMPLE 3.4. This example has a flower-like interface and the level-set function [14]

$$\varphi(x) = (x_1^2 + x_2^2)^2\{1 + 0.4\sin(6\arctan(x_2/x_1))\} - 0.3.$$

The exact solution is chosen as

$$u(x) = \begin{cases} \dfrac{\varphi(x)}{\beta^-} & \text{if } x \in \Omega^- \\ \dfrac{\varphi(x)}{\beta^+} & \text{if } x \in \Omega^+. \end{cases}$$

A typical Cartesian mesh for the interface problem is presented in Figure 13. Table 4 shows the error on different grids. In Figure 14, we plot the L^∞ error of MIFVE and IFVE method in the log–log scale versus the mesh size h. Figure 15 shows the MIFVE solutions with $N = 64$ for these two contrasting coefficients.

https://doi.org/10.1017/S1446181120000073 Published online by Cambridge University Press

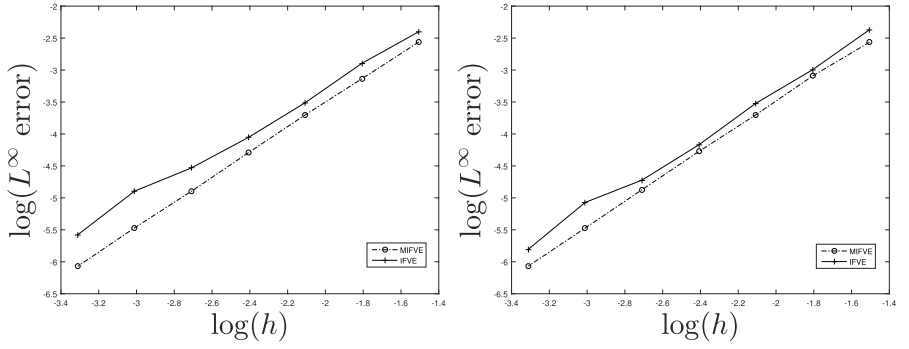

FIGURE 11. The L^∞ error under uniform refinement of the mesh for Example 3.3 with $(\beta^-, \beta^+) = (1, 10^4)$ (left) and $(\beta^-, \beta^+) = (10^4, 1)$ (right).

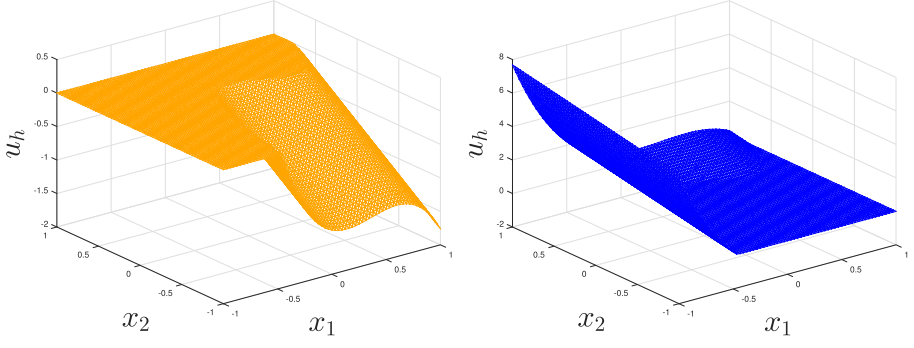

FIGURE 12. MIFVE solutions for Example 3.3 with $(\beta^-, \beta^+) = (1, 10^4)$ (left) and $(\beta^-, \beta^+) = (10^4, 1)$ (right).

TABLE 3. Errors of the MIFVE method for Example 3.3 with high coefficient contrasts.

Cases	N	L^∞ error	EO	L^2 error	EO	H^1 error	EO
$\beta^- = 1$	64	2.7495E-03	—	6.4299E-04	—	8.4430E-02	—
$\beta^+ = 10^4$	128	7.3210E-04	1.91	1.5699E-04	2.03	4.2123E-02	1.00
	256	1.9862E-04	1.88	4.0144E-05	1.97	2.1050E-02	1.00
	512	5.0794E-05	1.97	1.0085E-05	1.99	1.0507E-02	1.00
	1024	1.2679E-05	2.00	2.5124E-06	2.01	5.2534E-03	1.00
	2048	3.3927E-06	1.90	6.3434E-07	1.99	2.6245E-03	1.00
$\beta^- = 10^4$	64	2.7232E-03	—	1.5580E-03	—	2.0587E-01	—
$\beta^+ = 1$	128	8.0876E-04	1.75	3.8798E-04	2.01	1.0291E-01	1.00
	256	1.9899E-04	2.02	9.7074E-05	2.00	5.1436E-02	1.00
	512	5.3159E-05	1.90	2.4293E-05	2.00	2.5711E-02	1.00
	1024	1.3422E-05	1.99	6.0746E-06	2.00	1.2855E-02	1.00
	2048	3.3697E-06	1.99	1.5226E-06	2.00	6.4265E-03	1.00

https://doi.org/10.1017/S1446181120000073 Published online by Cambridge University Press

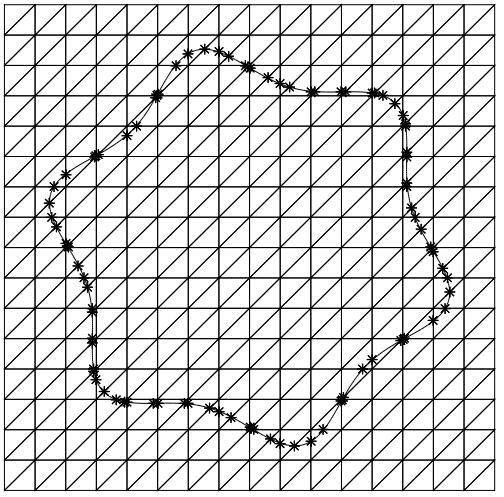

FIGURE 13. A typical Cartesian mesh for Example 3.4.

TABLE 4. Errors of the MIFVE method for Example 3.4 with high coefficient contrasts.

Cases	N	L^∞ error	EO	L^2 error	EO	H^1 error	EO
$\beta^- = 1$	64	2.7395E-03	—	1.2005E-03	—	7.9166E-02	—
$\beta^+ = 10^4$	128	8.1628E-04	1.75	2.8317E-04	2.08	3.9584E-02	1.00
	256	2.3158E-04	1.82	7.8718E-05	1.85	1.9589E-02	1.01
	512	5.7989E-05	2.00	1.9787E-05	1.99	9.7602E-03	1.01
	1024	1.4628E-05	1.99	5.3857E-06	1.88	4.8746E-03	1.00
	2048	3.8427E-06	1.93	1.4461E-06	1.90	2.4307E-03	1.00
$\beta^- = 10^4$	64	1.8939E-03	—	3.1155E-03	—	2.4508E-01	—
$\beta^+ = 1$	128	5.1095E-04	1.89	8.0779E-04	1.95	1.2256E-01	1.00
	256	1.1468E-04	2.16	1.8608E-04	2.12	6.1154E-02	1.00
	512	3.0088E-05	1.93	4.5673E-05	2.03	3.0560E-02	1.00
	1024	9.2734E-06	1.70	1.1196E-05	2.03	1.5276E-02	1.00
	2048	2.4782E-06	1.90	2.7630E-06	2.02	7.6361E-03	1.00

4. Conclusions

In this paper, we introduced a modified immersed finite volume element method for solving second-order elliptic interface problems with large discontinuous coefficient on nonbody fitted meshes. By reconstructing the control volume according to the interface, we can overcome the oscillating behaviour of the IFVE method. Furthermore, the new method has the same computational cost as the IFVE method, and it is easier than the IFVE method. Numerical results show that the new method has optimal convergence order in the H^1, L^2 and L^∞ norms. Further works related to the method are

https://doi.org/10.1017/S1446181120000073 Published online by Cambridge University Press

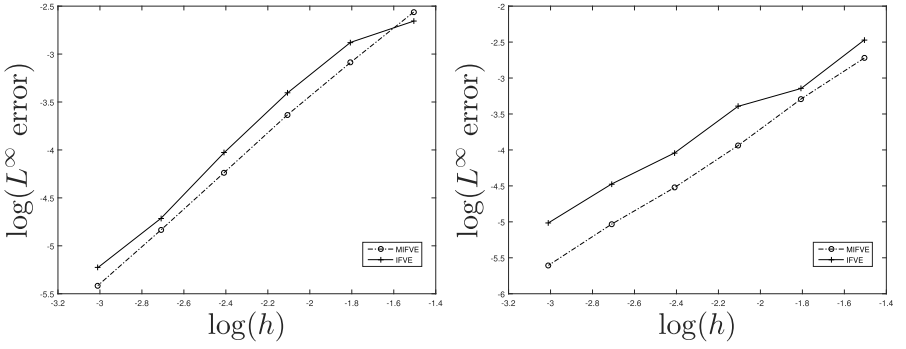

FIGURE 14. The L^∞ error under uniform refinement of the mesh for Example 3.4 with $(\beta^-, \beta^+) = (1, 10^4)$ (left) and $(\beta^-, \beta^+) = (10^4, 1)$ (right).

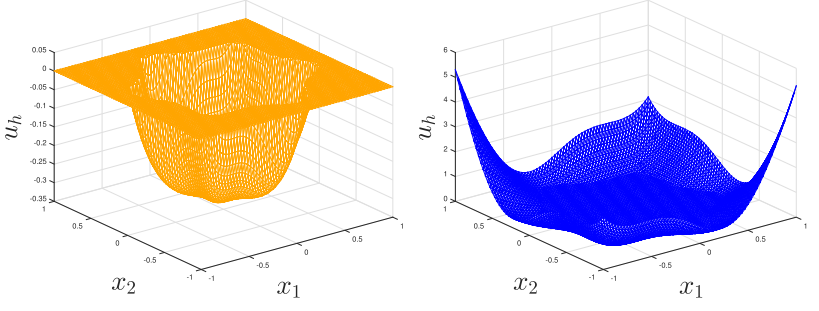

FIGURE 15. MIFVE solutions for Example 3.4 with $(\beta^-, \beta^+) = (1, 10^4)$ (left) and $(\beta^-, \beta^+) = (10^4, 1)$ (right).

elliptic interface problems with nonhomogeneous jumps, parabolic interface problems with a moving interface and planar elasticity interface problems.

Acknowledgements

This project is partially supported by the National Natural Science Foundation of China Nos. 11701283, 11971241, the Fundamental Research Funds for the Central Universities No. KJQN201839, Excellent Young Talents Science and Technology Fund of College of Engineering No. YQ 201607. The authors would like to thank the anonymous referees for their useful comments and suggestions which have helped to improve the paper greatly.

References

[1] N. An, X. Yu, H. Chen and H. Huang, "A partially penalty immersed Crouzeix–Raviart finite element method for interface problems", *J. Inequal. Appl.* **2017** (2017) 1–29; doi:10.1186/s13660-017-1461-5.

[2] J. Barrett, C. Elliott and M. Charles, "Fitted and unfitted finite-element methods for elliptic equations with smooth interfaces", *IMA J. Numer. Anal.* **52** (1987) 283–300; doi:10.1093/imanum/7.3.283.
[3] J. Bramble and J. King, "A finite element method for interface problems in domains with smooth boundaries and interfaces", *Adv. Comput. Math.* **6** (1996) 109–138; doi:10.1007/BF02127700.
[4] K. Brattkus and D. Meiron, "Numerical simulations of unsteady crystal growth", *SIAM J. Appl. Math.* **52** (1992) 1303–1320; doi:10.1137/0152075.
[5] R. Büger, R. Ruiz-Baier and C. Tian, "Stability analysis and finite volume element discretization for delay-driven spatio-temporal patterns in a predator–prey model", *Math. Comput. Simulation* **132** (2017) 28–52; doi:10.1016/j.matcom.2016.06.002.
[6] Z. Chen and J. Zou, "Finite element methods and their convergence for elliptic and parabolic interface problems", *Numer. Math.* **79** (1998) 175–202; doi:10.1007/s002110050336.
[7] C. Chen, W. Liu and C. Bi, "A two-grid characteristic finite volume element method for semilinear advection-dominated diffusion equations", *Numer. Methods Partial Differential Equations* **29** (2013) 1543–1562; doi:10.1002/num.21766.
[8] S. Chou, D. Kwak and Q. Li, "L^p error estimates and super convergence for covolume or finite volume element methods", *Numer. Methods Partial Differential Equations* **19** (2003) 463–486; doi:10.1002/num.10059.
[9] S. Chou and X. Ye, "Unified analysis of finite volume methods for second order elliptic problems", *SIAM J. Numer. Anal.* **45** (2007) 1639–1653; doi:10.1137/050643994.
[10] R. Ewing, Z. Li, L. Tao and Y. Lin, "The immersed finite volume element methods for the elliptic interface problems", *Math. Comput. Simulation* **50** (1999) 63–76; doi:10.1016/S0378-4754(99)00061-0.
[11] R. Ewing, L. Tao and Y. Lin, "On the accuracy of the finite volume element method based on piecewise linear polynomials", *SIAM J. Numer. Anal.* **39** (2002) 1865–1888; doi:10.1137/S0036142900368873.
[12] A. Fogelson, "A mathematical model and numerical method for studying platelet adhesion and aggregation during blood clotting", *J. Comput. Phys.* **56** (1984) 111–134; doi:10.1016/0021-9991(84)90086-X.
[13] F. Gao and Y. Yuan, "An upwind finite volume element method based on quadrilateral meshes for nonlinear convection-diffusion problems", *Numer. Methods Partial Differential Equations* **25** (2009) 1067–1085; doi:10.1002/num.20387.
[14] R. Guo, T. Lin and X. Zhang, "Nonconforming immersed finite element spaces for elliptic interface problems", *Comput. Math. Appl.* **75** (2018) 2002–2016; doi:10.1016/j.camwa.2017.10.040.
[15] A. Hansbo and P. Hansbo, "An unfitted finite element method, based on Nitsche's method, for elliptic interface problems", *Comput. Methods Appl. Mech. Engrg.* **47** (2002) 5537–5552; doi:10.1016/S0045-7825(02)00524-8.
[16] X. He, T. Lin and Y. Lin, "A bilinear immersed finite volume element method for the diffusion equation with discontinuous coefficient", *Commun. Comput. Phys.* **6** (2009) 185–202; doi:10.4208/cicp.2009.v6.p185.
[17] P. Huang, H. Wu and Y. Xiao, "An unfitted interface penalty finite element method for elliptic interface problems", *Comput. Methods Appl. Mech. Engrg.* **323** (2017) 439–460; doi:10.1016/j.cma.2017.06.004.
[18] K. Ito, K. Kunisch and Z. Li, "Level-set function approach to an inverse interface problem", *Inverse Problems* **17** (2001) 1225–1242; doi:10.1088/0266-5611/17/5/301.
[19] H. Ji, J. Chen and Z. Li, "A symmetric and consistent immersed finite element method for interface problems", *J. Sci. Comput.* **61** (2014) 533–557; doi:10.1007/s10915-014-9837-x.
[20] D. Kwak, S. Jin and D. Kyeong, "A stabilized P1-nonconforming immersed finite element method for the interface elasticity problems", *ESAIM Math. Model. Numer. Anal.* **51** (2017) 187–207; doi:10.1051/m2an/2016011.
[21] D. Kwak and J. Lee, "A modified P_1 immersed finite element method", *J. Pure Appl. Math.* **104** (2015) 471–494; doi:10.12732/ijpam.v104i3.14.

[22] D. Kwak, K. Wee and K. Chang, "An analysis of a broken P1-nonconforming finite element method for interface problems", *SIAM J. Numer. Anal.* **48** (2010) 2117–2134; doi:10.1137/080728056.
[23] B. Lamichhane and B. Wohlmuth, "Mortar finite elements for interface problems", *Computing* **72** (2004) 333–348; doi:10.1007/s00607-003-0062-y.
[24] R. LeVeque and Z. Li, "The immersed interface method for elliptic equations with discontinuous coefficients and singular sources", *SIAM J. Numer. Anal.* **31** (1994) 1019–1044; doi:10.1137/0731054.
[25] R. Li, Z. Chen and W. Wu, *Generalized difference methods for differential equations: numerical analysis of finite volume methods* (Dekker, New York, 2000); doi:10.1201/9781482270211.
[26] Z. Li, T. Lin, Y. Lin and R. Rogers, "An immersed finite element space and its approximation capability", *Numer. Methods Partial Differential Equations* **20** (2004) 338–367; doi:10.1002/num.10092.
[27] Z. Li, T. Lin and X. Wu, "New Cartesian grid methods for interface problems using the finite element formulation", *Numer. Math.* **96** (2003) 61–98; doi:10.1007/s00211-003-0473-x.
[28] T. Lin, Y. Lin and X. Zhang, "A method of lines based on immersed finite elements for parabolic moving interface problems", *Adv. Appl. Math. Mech.* **5** (2013) 548–568; doi:10.4208/aamm.13-13S11.
[29] T. Lin, Y. Lin and X. Zhang, "Partially penalized immersed finite element methods for elliptic interface problems", *SIAM J. Numer. Anal.* **53** (2015) 1121–1144; doi:10.1137/130912700.
[30] T. Lin, D. Sheen and X. Zhang, "A nonconforming immersed finite element method for elliptic interface problems", *J. Sci. Comput.* **79** (2019) 442–463; doi:10.1007/s10915-018-0865-9.
[31] T. Lin and X. Zhang, "Linear and bilinear immersed finite elements for planar elasticity interface problems", *J. Comput. Appl. Math.* **236** (2012) 4681–4699; doi:10.1016/j.cam.2012.03.012.
[32] C. Peskin, "Flow patterns around heart valves: a numerical method", *J. Comput. Phys.* **10** (1972) 252–271; doi:10.1016/0021-9991(72)90065-4.
[33] C. Peskin, "Numerical analysis of blood flow in the heart", *J. Comput. Phys.* **25** (1977) 220–252; doi:10.1016/0021-9991(77)90100-0.
[34] S. Unverdi and G. Tryggvason, "A front-tracking method for viscous, incompressible, multi-fluid flows", *J. Comput. Phys.* **100** (1992) 25–37; doi:10.1016/0021-9991(92)90307-K.
[35] H. Wang, J. Chen, P. Sun and N. Wang, "A conforming enriched finite element method for Stokes interface problems", *Comput. Math. Appl.* **75** (2018) 4256–4271; doi:10.1016/j.camwa.2018.03.027.
[36] Q. Wang and Z. Zhang, "A stabilized immersed finite volume element method for elliptic interface problems", *Appl. Numer. Math.* **143** (2019) 75–87; doi:10.1016/j.apnum.2019.03.010.
[37] Q. Wang, Z. Zhang and Z. Li, "A Fourier finite volume element method for solving two-dimensional quasi-geostrophic equations on a sphere", *Appl. Numer. Math.* **71** (2013) 1–13; doi:10.1016/j.apnum.2013.03.007.
[38] Q. Wang, Z. Zhang, X. Zhang and Q. Zhu, "Energy-preserving finite volume element method for the improved Boussinesq equation", *J. Comput. Phys.* **270** (2014) 58–69; doi:10.1016/j.jcp.2014.03.053.
[39] T. Wang, "Alternating direction finite volume element methods for 2D parabolic partial differential equations", *Numer. Methods Partial Differential Equations* **24** (2008) 24–40; doi:10.1002/num.20224.
[40] X. Wang and Y. Li, "L^2 Error estimates for high order finite volume methods on triangular meshes", *SIAM J. Numer. Anal.* **54** (2016) 2729–2749; doi:10.1137/140988486.
[41] L. Zhu, Z. Zhang and Z. Li, "An immersed finite volume element method for 2D PDEs with discontinuous coefficients and non-homogeneous jump conditions", *Comput. Math. Appl.* **70** (2015) 89–103; doi:10.1016/j.camwa.2015.04.012.